Figure 1. A. Multivariable Association of Putative Pathogenic Rare Variant Carrier Status with QTc Interval Across Tertiles of QTc Polygenic Risk Score. B. Top PRS Decile and Monogenic Mutation Carrier Proportions Across QTc Strata. Multivariable models were adjusted for age, sex, beta blocker therapy, calcium channel blocker therapy and first 12 principal components. Interaction analysis was performed by including an interaction term (prs tertile * carrier status) in the multivariable model; LQTS: Long QT Syndrome; PRS: Polygenic Risk Score;LQTS genes included: KCNQ1, KCNH2, SCN5A, KCNJ2, KCNE2, CACNA1C, CAV3, TRDN, ANK2.

B-YIA1-03

DEVELOPMENT AND VALIDATION OF A MULTI-VARIABLE MODEL FOR REAL-TIME PREDICTION OF CARDIAC ARREST AND OTHER CARDIOVASCULAR (CV) COMPLICATIONS IN HOSPITALIZED PATIENTS WITH COVID-19

Julie K. Shade BS, Ashish N. Doshi MD, PhD, Eric Sung BA, Dan M. Popescu BS, Anum S. Minhas MD, Nisha A. Gilotra MD, Konstantinos N. Aronis MD, Allison G. Hays MD and Natalia A. Trayanova PhD, FHRS

Background: CV manifestations of COVID-19 carry significant morbidity and mortality. Currently, risk prediction for adverse CV events is limited, and existing approaches fail to account for the dynamic course of the disease.
**Objective:** To develop and validate the COVID-HEART predictor, a novel continuously-updating risk prediction technology, to forecast CV complications in hospitalized patients with COVID-19.
Methods: Vital sign, laboratory, and electrocardiographic data from 2555 and 1855 COVID-19 patients were used to train COVID-HEART to predict cardiac arrest and imaging-confirmed thromboembolic events, respectively. To assess the predictor's performance in the face of rapidly changing clinical treatment guidelines, it was tested on 1103 and 796 patients hospitalized after the end of data collection for the development set (Fig.1A).
Results: In testing, the COVID-HEART predictor achieved areas under the receiver operating characteristic curve (AUROCs) of 0.906 and 0.768, sensitivities of 0.788 and 0.833, and specificities of 0.890 and 0.818 for prediction of cardiac arrest and thromboembolic events, respectively (Fig.1B-C). The respective median test early warning times were 20.5 and 36 hours. Over 20 iterations of temporally-divided testing, the respective mean AUROCs were 0.920 (95% CI: 0.916-0.923) and 0.765 (95% CI: 0.743-0.787).
Conclusion: COVID-HEART is fully transparent and can thus identify predictive features for each outcome derived from clinical data inputs (Fig.1D-E). It is anticipated to provide tangible clinical

decision support in triaging patients and optimizing resource use, with its potential clinical utility extending beyond COVID-19.
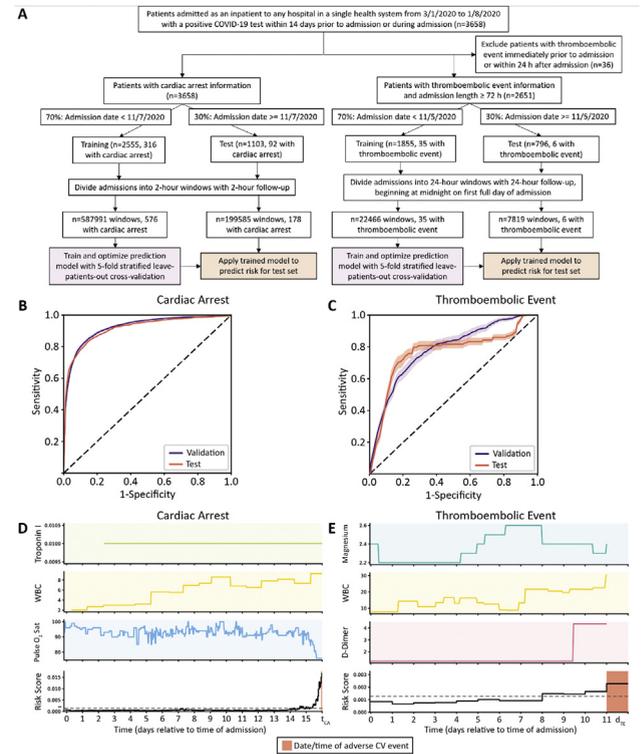
ABSTRACT B-YIA2:
Young Investigator Competition - Basic Finalists

Wednesday, June 30, 2021
10:30 am - 11:30 am

B-YIA2-01

MECHANO-ARRHYTHMOGENICITY IS ENHANCED IN LATE REPOLARISATION DURING ISCHEMIA AND DRIVEN BY A TRPA1-, CALCIUM-, AND REACTIVE OXYGEN SPECIES-DEPENDENT MECHANISM

Breanne Ashleigh Cameron BS and T. Alexander Quinn PhD

Background: Cardiac dyskinesis during ischemia results in arrhythmias *via* mechanically-induced changes in electrophysiology ('mechano-arrhythmogenicity'). While cellular mechanisms of mechano-arrhythmogenicity are unknown, ischemic alterations in voltage-Ca^{2+} dynamics may create a vulnerable period (VP) for mechano-arrhythmogenicity during late repolarisation.
Objective: Determine cellular mechanisms of mechano-arrhythmogenicity in ischemia and define the importance of the VP.
Methods: Rabbit LV myocytes were paced at 1Hz and rapidly stretched (10-18% increase in sarcomere length over ~110ms) during diastole or the VP in control (CTL) or simulated ischemic (SI) conditions. Drugs were used to buffer Ca^{2+} (BAPTA), stabilise ryanodine receptors (dantrolene), block mechano-sensitive TRPA1 (HC-030031) or K_{ATP} channels (glibenclamide), or to chelate (NAC), block (DPI), or increase (fluorophore photoexcitation) reactive oxygen species (ROS) production. Voltage-Ca^{2+} dynamics were simultaneously monitored by dual fluorescence imaging with a single camera-optical splitter system to assess the VP ($= Ca^{2+}$ transient - action potential duration). Diastolic Ca^{2+} was measured with ratiometric imaging.
Results: The VP was longer in SI than CTL (146$\pm$7 *vs* 54$\pm$8ms; $n=50$ cells, $N=6$ rabbits; $p<0.0001$). Mechano-arrhythmogenicity

during the VP was greater in SI compared to CTL (7 *vs* 1% of stretches induced arrhythmias; $n=50$, $N=6$; $p<0.005$) but was similar in diastole. Arrhythmias during the VP were more complex than in diastole (100 *vs* 69% had sustained activity; $n=50$, $N=6$; $p<0.05$). In the VP, arrhythmia incidence was reduced by BAPTA (2%; $p<0.05$), HC-030031 (1%; $p<0.005$), NAC (1%; $p<0.005$), or DPI (2%; $p<0.05$), while dantrolene had no effect. Fluorophore photoexcitation caused an increase during both the VP and diastole (29 and 14%, $n=42$, $N=4$; $p<0.05$). Glibenclamide reduced the size of the VP (109 ± 6ms; $p<0.0001$), with an associated decrease in arrhythmia incidence (2%, $n=50$, $N=6$; $p<0.05$). SI increased diastolic Ca^{2+} ($9\pm1\%$, $n=25$, $N=5$; $p<0.0001$), which was not prevented by NAC or HC-030031.
Conclusion: Mechano-arrhythmogenicity in ischemia is enhanced during the VP and involves TRPA1, Ca^{2+}, and ROS, representing potential anti-arrhythmic targets.

B-YIA2-02

CELLULAR AND ELECTROPHYSIOLOGICAL CHARACTERIZATION OF TRIADIN KNOCKOUT SYNDROME USING HUMAN INDUCED PLURIPOTENT STEM CELL-DERIVED CARDIOMYOCYTES

Daniel J. Clemens BS, Dan Ye MD, Lili Wang PhD, Changsung John Kim PhD, Wei Zhou, Steven Michael Dotzler BA, David Tester BS, Isabelle Marty, Bjorn C. Knollmann MD, PhD and Michael John Ackerman MD, PhD

Background: Triadin knockout syndrome (TKOS) is a malignant arrhythmia disorder caused by recessive null variants in *TRDN*-encoded cardiac triadin. TKOS is characterized by QT prolongation, T-wave inversions in the precordial leads, ectopy upon stress testing, and a severe disease expression of cardiac arrest in childhood.
Objective: To characterize the cellular and electrophysiological phenotype of TKOS using induced pluripotent stem cell-derived cardiomyocytes (iPSC-CMs).
Methods: iPSC-CMs were generated from two unrelated patients with TKOS and an unrelated control (TKOS Patient 1: p.D18fs*13/ D18fs*13; TKOS Patient 2: p.N9fs*5/K147fs*0). CRISPR/Cas9 was used to insert homozygous p.D18fs*13 into a different healthy control line thereby generating a patient-independent TKOS model (TRDN-/-) and isogenic control iPSC-CMs. Protein expression was measured using immunofluorescence. Action potential duration (APD) and L-type calcium channel (LTCC) properties were measured by whole cell patch-clamp. Calcium handling was assessed using Fluo-4 calcium indicator.
Results: APD90 was prolonged significantly from 507 ± 20 ms ($n=9$) in the unrelated control to 662 ± 62 ms ($n=9$; $P<0.05$) in TKOS Patient 1 and 653 ± 39 ms ($n=9$; $P<0.05$) in TKOS Patient 2. This was confirmed in TRDN-/- iPSC-CMs compared to isogenic control (518 ± 27 ms, $n=17$ vs. 312 ± 20 ms, $n=16$; $P<0.0001$). Additional work in TRDN-/- iPSC-CMs revealed that loss of triadin underlies decreased expression and co-localization of RyR2 and Casq2 leading to slow and decreased calcium release from the sarcoplasmic reticulum. These abnormal calcium transients lead to slow inactivation of the LTCC which contributes to the observed APD prolongation. Finally, these changes underlie frequent cellular arrhythmias including early- and delayed afterdepolarizations and APD alternans.
Conclusion: Here, we characterized the first set of iPSC-CM models of TKOS and provide further evidence for recessive null variants in *TRDN* as a self-sufficient monogenetic substrate for potentially lethal genetic heart disease. These cells display APD prolongation, calcium handling abnormalities, and arrhythmias which likely underlie the unique clinical and arrhythmogenic phenotype observed in patients with TKOS.

B-YIA2-03

A GOVERNING EQUATION TO EXPLAIN THE NUMBER OF WAVELETS AND ROTORS OBSERVED IN HUMAN VENTRICULAR FIBRILLATION

Dhani Dharmaprani BEng, Christopher Bradley, Martin Hayward, David Paterson, Peter Taggart, Evan Jenkins BEng, Jing Xian Quah, Anandaroop Lahiri MBBS, MD, Kathryn Tiver, Lewis Mitchell, Richard H. Clayton PhD, Martyn P. Nash PhD and Anand N. Ganesan MBBS, CCDS, CEPS-A

Backgroundbackground: VF is commonly characterised by two mechanisms, multi wavelet reentry and rotors, but no governing equation exists to explain and predict their population dynamics.
Objective: We hypothesized a single equation derived from an M/G/∞ renewal process could explain rotor and wavelet numbers in VF.
Methodsmaterials-methods: Phase singularity (PS) and wavefront (WF) tracking was used to identify wavelets and rotors in epicardial recordings of induced VF during cardiac surgery ($n=13$ patients). Autocorrelation and distributions of PS and WF lifetimes and inter-formation times were assessed to verify an underlying renewal process. Distributions were fitted using maximum likelihood to calculate formation (λ_f) and destruction (λ_d) rates, and combined in an M/G/∞ process to develop a potential governing equation of VF dynamics.
Results: PS and WF inter-event-time distributions were consistent with the Weibull in all 210 epochs (PS: mean X^2 $P=0.23$(95%CI,0.18,0.28); WF: mean X^2 $P=0.19$(95% CI,0.13,0.27)), with zero autocorrelation at non-zero lags, indicative of an underlying renewal process over all stages (perfusion, ischemia and reflow). The M/G/∞ equation accurately predicted average PS and WF number (R>0.90) and population distribution (X^2 P>0.05) in all epochs. Differences in λ_f (term: 0.015/ms (95%CI,0.010,0.020), non-term 0.023/ms (95% CI,0.019,0.027)), and average PS number (term: 1.68 (95%CI, 1.36, 2.00), non-term: (2.00 (95%CI, 1.86, 2.15)) was observed in spontaneous VF termination.
Conclusion: M/G/∞ renewal process provides a governing equation to explain the number of wavelets and rotors in VF, which could be used in mechanistic studies to guide development of new therapies.

Governing equation accurately predicts PS and wavefront population dynamics in VF